

See discussions, stats, and author profiles for this publication at: <https://www.researchgate.net/publication/221801224>

Orientation of a Dispersion of Kaolinite Flowing in a Jet

ARTICLE *in* LANGMUIR · FEBRUARY 2012

Impact Factor: 4.46 · DOI: 10.1021/la204864p · Source: PubMed

READS

46

3 AUTHORS, INCLUDING:



[Junaid Qazi](#)

The University of Calgary

12 PUBLICATIONS 73 CITATIONS

[SEE PROFILE](#)



[J. K. Cockcroft](#)

University College London

84 PUBLICATIONS 1,208 CITATIONS

[SEE PROFILE](#)

Orientation of a Dispersion of Kaolinite Flowing in a Jet

S. Junaid S. Qazi*,†,‡ and Adrian R. Rennie

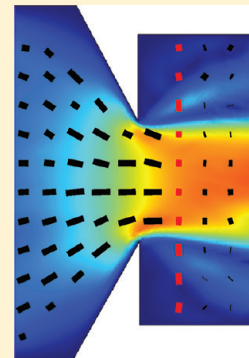
Department of Physics and Astronomy, Uppsala University, Box 516, S-751 20 Uppsala, Sweden

Jeremy K. Cockcroft

Department of Chemistry, University College London, 20 Gordon Street, London WC1H 0AJ, United Kingdom

Supporting Information

ABSTRACT: Orientational alignment in a dilute dispersion of kaolinite particles has been investigated in a flow pattern that combines both shear and elongational stress, namely flow at a jet created by a 2 mm diameter nozzle inserted in a 6 mm diameter pipe. Spatially-resolved X-ray diffraction with synchrotron radiation permits detailed maps of the alignment to be deduced and compared with fluid mechanics calculations of the flow. The angular distribution of diffracted intensity from a given position in the pipe provides information about the orientation distribution of the particles. This is quantified and presented in terms of order parameters. The cone-shaped nozzle provides a jet of liquid giving a high degree of alignment of the particles that is uniform along lines across the conical section and constant in the small straight-sided region at the exit of the nozzle. The vortex motion that arises from the flow with a modest Reynolds number could be determined as well as the tendency for some particles to align with their large faces perpendicular to the overall flow direction at the flat surface of the nozzle outlet.



INTRODUCTION

Applications of complex fluids such as colloidal dispersions and polymers in concentrated solutions or melts often require flow processing. In many practical cases, flows involve constrictions or other geometry that can cause large elongational components of the strain. For example, printing technology for materials and devices¹ with inkjets requires dispersed pigment² to pass through a fine nozzle. This process allows the active materials to be deposited precisely where they are needed and is attracting considerable interest. Low cost electronic devices, even on flexible substrates, can be fabricated. The direct printing of electronic circuits with conducting polymers has been reported with high-resolution inkjet printers.³ Coating of paper requires rapid flow of a colloidal dispersion through a very narrow gap between a blade and a rapidly moving paper surface.^{4,5} Understanding the flow patterns as well as the properties of fluids under these conditions is crucial for the development of new materials. For these reasons, studies of structure and orientation of particles in elongational and nonuniform flow are important.

Even dilute dispersions are often characterized by measurements in nonuniform flow fields. For example, capillary viscometry involves flow through pipes with changes of diameter. Rheology of pastes⁶ and the structures that arise in colloidal dispersion under flow in different geometries are described widely.^{7,8} Most studies have been made with spherical particles in simple geometries that cause shear flow: these have demonstrated changes from a distorted crystal to sliding layers,⁹ a transition from three to two-dimensional order¹⁰ and one-dimensional strings.¹¹ Plate-like anisotropic particles including clay minerals have shown orientational

ordering in a Couette^{12,13} cell and under pipe flow¹⁴ where the effects of bends in pipe on ordering have been discussed. A number of experiments have used small-angle scattering^{12,13,15,16} to study orientation but for crystalline particles there are advantages in use of diffraction as it can be used to determine the full orientation distribution. Such experiments have been reported using both neutron¹⁵ and X-ray diffraction.^{16,17} Measurements of rheology using either Couette or cone-on-plate geometry involve flow between small gaps, and it is very useful to understand how samples respond to these constraints.^{18,19}

Alignment induced by elongational flow has been reported for mixed surfactant mesophases^{20,21} in studies using an “opposing jet” elongational flow cell. More recent studies²² on a well-characterized colloidal dispersion of plate-like, nickel hydroxide particles with a diameter of 120 nm have shown that extensional strain rates of the order of 16 s^{-1} can effectively induce alignment of the small particles (23 wt %). A more concentrated dispersion (60 wt %) of similar particles has not shown alignment under shear at strain rates up to 6000 s^{-1} in a Couette cell.²³

In a previous paper,²⁴ we have described the flow of a dilute dispersion of kaolinite particles in a uniform pipe using the technique of high-energy synchrotron X-ray diffraction. High spatial resolution of the order of $20 \mu\text{m}$ enabled the investigation of a range of effects of the wall on flow in a pipe of 5 mm internal diameter. The small size of the incident

Received: May 1, 2011

Revised: January 31, 2012

Published: February 2, 2012



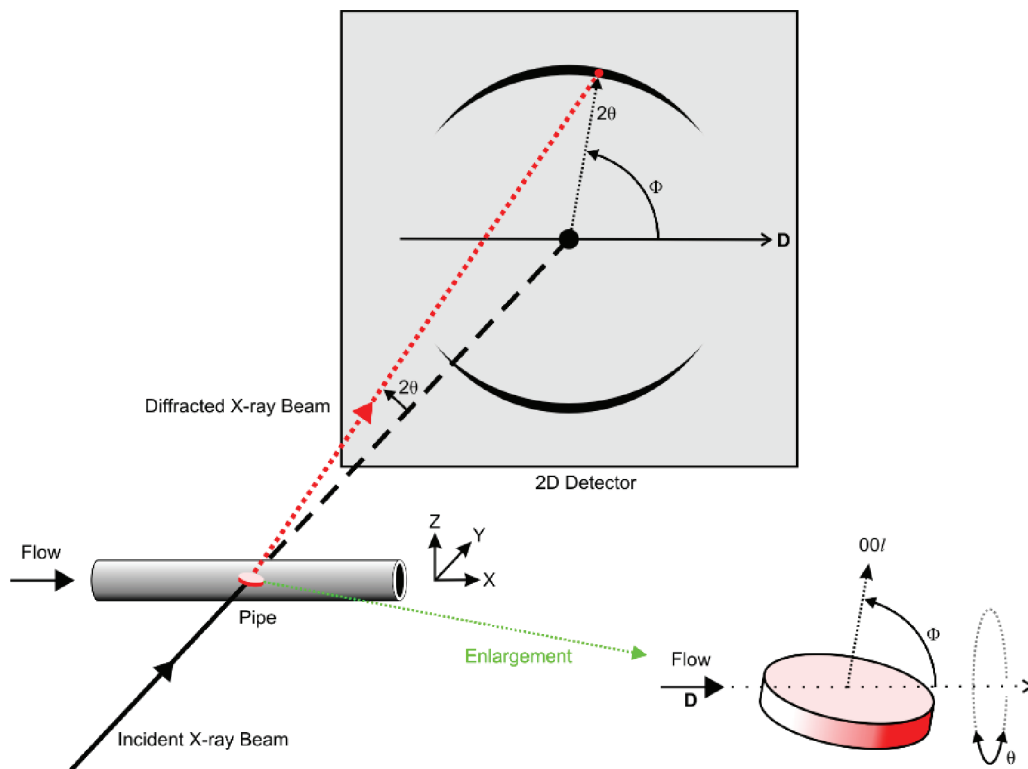


Figure 1. Schematic diagram of diffraction from one single-crystal, plate-like particle. Diffraction such as that from the 001 spacing can be related to the orientation of the particle. For the particle that is aligned as shown, the 001 peaks appear at about $\Phi = 90^\circ$ and 270° . An assembly of randomly oriented particles would give a uniform ring of intensity. The intensity for a distribution of aligned particles is also shown. A line perpendicular to that joining the maxima of the two arcs of diffraction defines a direction of preferential orientation that can be compared with the director, D , that is in the flow direction.

beam makes this method very suitable for studies of complex geometry and nonuniform flow. In the present paper, we provide data on the alignment of a kaolinite dispersion as it flows through a constriction in a pipe to form a jet. Apart from the elongational stress in the nozzle, the flow creates a vortex because of the change in Reynolds number at the outlet. The effects of the constriction on the flow alignment and the range of reorientation of plate-like particles at the nozzle outlet will be presented. The theoretical concepts and the experimental arrangement are similar to those described in detail in the previous article.²⁴ Alignment of anisotropic objects and liquid crystals is often conveniently described by order parameters that are weighted averages of the orientation distribution.²⁵ Such approaches can be applied to scattering experiments as the angular distribution of the scattering is related directly to the orientation of the material. Several papers describe how this can be applied to small-angle scattering and diffraction of polymers^{26–28} and particles.^{16,24} Results are described with respect to a director. In the cone inlet, the director is selected by using an automatic algorithm for each measured data set and is taken in the direction of the local velocity. The extent of flow-induced alignment in the cone inlet is compared with the fluid dynamics calculations in our discussions. The selection of an overall director, D , is similar to that in used our previous paper²⁴ and is in the direction of the axis of the pipe which is also the flow direction.

Diffraction from a Model plate-like Particle Oriented under Flow. Diffraction from crystalline particles is described by the Bragg equation, $\lambda = 2d \sin \theta$, where λ is the wavelength of the incident beam, d is the separation between atomic planes,

and θ is the angle between incident beam and planes of scattering atoms. If the crystals are randomly oriented, then the diffraction observed on a two-dimensional detector will be an isotropic ring of uniform intensity. Preferential orientation of the particles gives rise to anisotropic intensity in the diffraction ring and provides information about the distribution of the alignment of the particles. A schematic diagram (Figure 1) shows a plate that is oriented with the normal to its large face parallel to the incident beam. This alignment of a crystal would give a 001 diffraction spot on the detector. To satisfy the diffraction condition, the crystal must be tilted by θ (half the Bragg angle 2θ) with respect to the incident beam. As this amounts to only 1.06° , this is small compared with the angular distribution. If a large number of such particles have a distribution of orientation about a particular direction, then arcs of the diffraction ring will appear as shown in Figure 1. The direction that joins the maxima of the diffraction can be taken to determine a vector, D , that is used to quantify the alignment distribution in terms of order parameters. For disk-like particles, the diameters tend to align parallel to the flow. The unique orientation for a cylindrical pipe is along the axis, and it is convenient to discuss the distribution of intensity with respect to a line that is perpendicular to the flow direction.

Averages of the diffraction intensity that are weighted by even Legendre polynomials can be taken as order parameters. These are used widely in the study of liquid crystalline materials.²⁵ Specifically, S_2 is calculated using the first even Legendre polynomial $P_2(\sin \Phi)$ as in ref 24. In a geometry where the flow direction varies, it is sometimes useful to consider order parameters that are calculated with respect to

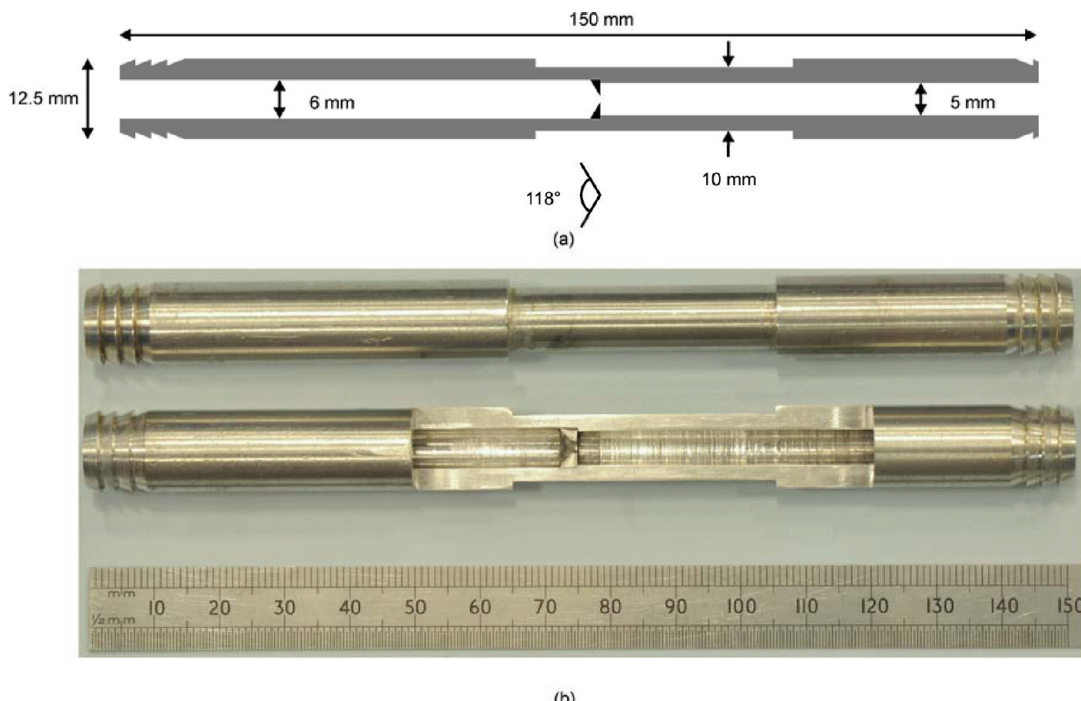


Figure 2. (a) Diagram of the pipe with a 2 mm nozzle. (b) Photograph of the straight pipe without constriction as used previously plus the pipe with a 2 mm jet used in these experiments that has been sectioned to its midline. The wall thickness at the scanned area was 2.5 mm, and the cone angle of the nozzle was nominally 118°.

the local flow direction rather than an overall direction. For the region of inlet to the nozzle, we will present the order parameter S_{2L} that is calculated with respect to the local velocity direction.

EXPERIMENTAL SECTION

Sample Preparation and Diffraction Experiments. The sample consisted of kaolinite particles dispersed at 8 wt % in water. Dynamic light scattering and electron microscopy indicated that the mean diameter of the large face of the particles was in the range 1–2 μm and that the mean thickness was $\sim 0.1 \mu\text{m}$. Assuming the density of kaolinite to be 2.62 g cm^{-3} , 8 wt % is ~ 3 vol %. This is below the overlap concentration that is estimated to be above 5 vol % for these particles according to the formula of Jorgenson and Zukoski.¹⁶ The sample is thus below the minimum concentration at which the rotational motion of the anisotropic particles is restricted directly by interparticle crowding. Details of the sample preparation are described elsewhere.²⁹ Dried kaolinite was used as received from Sigma-Aldrich. A dispersion of kaolinite in water is not stable because the opposite charges on the edges and faces of the particles at pH 7 cause flocculation and gelation.³⁰ To stabilize the particles, 0.5 wt % sodium polyacrylate with a molecular mass of 4000 g mol⁻¹ (grade N40, as provided by Ciba Chemicals, UK) was added to the dispersion. The low molecular mass of the stabilizer implies that the thickness of this adsorbed layer is negligible in terms of the overall particle dimensions. No changes were observed in the dispersion during the course of the measurements that took more than 24 hrs.

Diffraction measurements were made at the ID11 beamline of the European Synchrotron Radiation Facility (ESRF), Grenoble France.³¹ Photons with energy of 46.8 keV that corresponds to a wavelength of 0.265 Å were used. A small beam size 20 $\mu\text{m} \times 20 \mu\text{m}$ was obtained on the sample by using a combination of slits and refractive lenses.³² The incident beam was perpendicular to the pipe and hence the flow direction. The sample was translated along the horizontal (X) and vertical (Z) directions (see Figure 1) using an XYZ stage to obtain a two-dimensional map of alignment profile of kaolinite particles under flow. Apart from the flow geometry, all other experimental details

including the sample, pump, X-ray beam, diffractometer, and detector were identical to those described in the previous paper.²⁴

Flow Geometry. A drawing of the aluminum pipe used in the present study is shown in Figure 2. Aluminum was chosen for the pipe material as it is easy to machine and is structurally rigid. Unlike heavier metals, the absorption coefficient for X-rays is low. Alternative designs of flow cells fabricated from polymers showed significant distortion at the pressures required to establish rapid flow. The disadvantage of Bragg diffraction peaks from the pipe could be overcome by masking them in the analysis procedures. The inlet side has an internal diameter of 6 mm, and the outlet side has an internal diameter of 5 mm. At the center of the pipe, there is a 2 mm constricting nozzle with a nominal opening angle of 118° that was fabricated separately and inserted through the inlet side of the pipe. The opening is the usual angle made with high-speed steel drill bits. A photograph of the pipe used sectioned to its midline is shown in Figure 2b. The pipe was mounted with the flow axis horizontal on the diffractometer. The overall flow rate was maintained at 5 $\text{cm}^3 \text{s}^{-1}$ with a recirculating pump. This gives an average velocity of 0.2 m s^{-1} at the inlet, 1.6 m s^{-1} at the nozzle, and 0.25 m s^{-1} at the outlet. The velocities vary as the cross-sectional area of the pipe is different at each position in the pipe. However, the average velocity at the nozzle is similar to that used in the previous study of flow of similar dispersion in a uniform pipe with internal diameter 5 mm.²⁴

The diffraction from the sample under flow was measured at different positions in the pipe by making two-dimensional raster scans of the pipe through the incident beam. Coarse scans were made initially to obtain an overall picture of the flow with steps of 0.5 mm in each direction. Near the nozzle, scans were made with a finer raster of 50 $\mu\text{m} \times 100 \mu\text{m}$ in the horizontal (X) and vertical (Z) directions, respectively.

Data Analysis. The intensity from the 001 diffraction ring from kaolinite is evaluated as a function of azimuthal angle Φ . This directly provides information about the distribution of the normals to the large faces of the clay particles with respect to the flow direction. The details of the data analysis have been presented in the previous paper.²⁴ A statistical algorithm was used to remove single-crystal diffraction spots that arise from the grains of aluminum that form the pipe. The data are

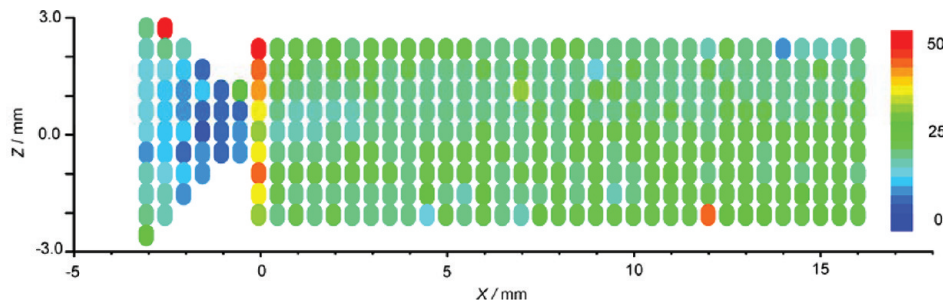


Figure 3. The 001 peak intensity averaged over all Φ for each data set in a two-dimensional scan is shown for different positions in the pipe, normalized for sample thickness at each point. The intensity at each point is proportional to the number of particles oriented with the normal to their large face in the XZ plane.

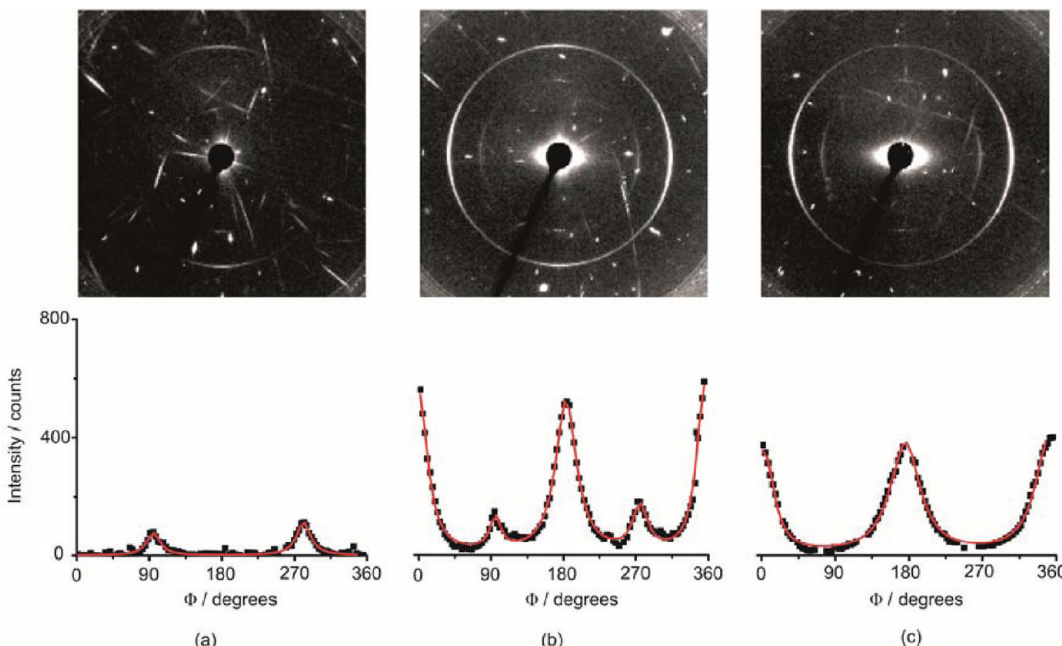


Figure 4. Diffraction intensity for the 001 peak shown in the raw data images (upper row) is plotted (below) as a function of azimuthal angle, Φ , at three different positions in the pipe: (a) on the axis just before the nozzle opening at $X = -0.15$ mm, $Z = 0.0$ mm, (b) on the axis at the nozzle opening, $X = 0.0$ mm, $Z = 0.0$ mm, (c) and to the side of the nozzle opening at $X = 0.05$ mm, $Z = -1.8$ mm. The red lines are the Lorentzian functions fitted to the data. Two strong peaks at $\Phi = 0^\circ$ and 180° that arise from particles perpendicular to the flow direction appeared in (b) which are not present in (a). The data acquisition time for each diffraction pattern is 60 s, and the plotted data points are obtained after background subtraction and masking.

presented graphically, and a number of quantitative parameters are derived that can be used to compare with fluid dynamics calculations. Data for the 001 intensity as a function of the azimuthal angle Φ were obtained for each point in the raster scan. These can be plotted directly and used for further analysis. Comparisons of intensity require correction for the path length of the sample in the beam that varies from point to point because of the cylindrical geometry of the pipe and the constriction.

As mentioned earlier, the selection of the director is different around the nozzle as compared to other positions where it is selected along the axis of the pipe as in our previous article.²⁴ In the cone, the director is determined for each individual diffraction pattern. The direction of orientation of the particles is readily obtained by a simple algorithm that finds the peaks of intensity for the 001 Bragg reflection from the kaolinite as a function of Φ . A line along the direction of these maxima can be taken as the director for subsequent calculations of the order parameters. The data can also be presented as plots of intensity in particular sectors of Φ , and these correspond to the fraction of particles oriented in those directions as described in the next section.

The Bragg angle, 2θ , for the 001 reflection of kaolinite is 2.12° with $\lambda = 0.265$ Å. Particles with large faces that are oriented at 1.06° away from the incident beam will satisfy the diffraction condition. However, this offset is small as compared to the spread of orientations observed in our experiments and can be neglected in our discussion.

RESULTS AND DISCUSSION

We present our results in four parts. First, the overall picture of the alignment of kaolinite particles over a large region of the pipe is presented with the help of data from an initial coarse scan of the entire pipe. Data from measurements with better spatial resolution near the constriction are then presented, and the orientation distribution of particles at different positions near the nozzle is described. In the third part, the alignment of the particles is compared with fluid dynamics calculations of the flow. Finally, the behavior of the kaolinite dispersion is described at the nozzle opening, which is the region where the largest effects are observed.

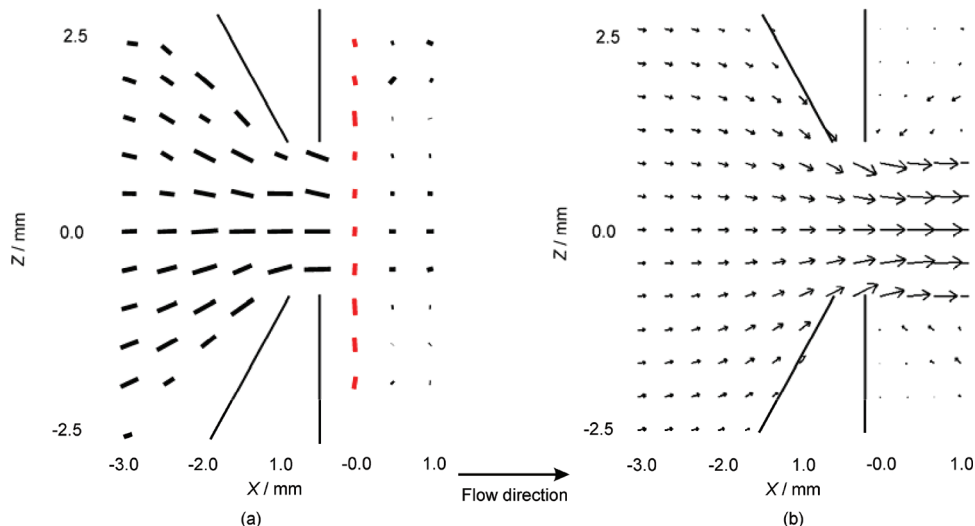


Figure 5. (a) Values of S_{2L} in the conical region of the nozzle obtained from the diffraction data. The lines are along the director selected individually for each measured position and the length of each line represents the extent of alignment for an individual data set. The maximum length of the line corresponds to $S_{2L} = 0.88$, and the smallest line indicates $S_{2L} = 0.26$. (b) Fluid dynamics calculations of the local velocity in the cone for a Newtonian fluid. The length of each arrow is proportional to the local velocity and the direction of arrows are in the flow direction.

Variation of Alignment. For a cylindrical pipe, the chord length corresponds to the sample thickness at a particular position. The chord-normalized intensity for the 001 kaolinite diffraction peak for the initial coarse scan is shown in Figure 3 to present an overall picture of the alignment of particles in the pipe. The intensity is averaged over all Φ and so for each position is a measure of the number of particles oriented with the normal to their large face in the XZ plane. The path length of the aluminum in the beam also changes with the position of the measurements. Especially in the region of the constriction, there is more aluminum in the beam and this amount increases from the conical inlet to the outlet with its 2 mm diameter opening within a thick region of metal. This gives rise to more bright spots of diffraction from single-crystal grains of aluminum. The total scattered intensity of a diffraction peak on the detector is directly related to the amount of sample in the beam in the absence of multiple scattering. The most interesting regions are the cone inlet, the nozzle, and the nozzle outlet. These are the regions where the significant variation in the normalized intensity is observed in Figure 3. The average velocities for these regions are 0.2, 1.6, and 0.25 m s^{-1} , respectively.

The variation of the chord-normalized intensity is indicative of changes in the alignment of the particles, but it is difficult to quantify the orientation with the help of the intensity alone. A more extensive analysis of order parameters is presented below to describe the extent of alignment.

Orientation Distributions in the Flow. The orientation of the particles is directly related to the anisotropy of the diffraction intensity. Figure 4 shows the rings of 001 diffraction as plots of intensity against Φ for three positions typical of the different regions in the flow. The full two-dimensional diffraction data for these positions are shown in Figure S1 of the Supporting Information. Our analysis focuses on the distribution of the intensity of the 001 kaolinite diffraction, and data for an annulus corresponding to $2\theta = 2.06 \pm 0.03^\circ$ on the detector are shown in Figure 4.

The distribution of 001 peak intensity and particle orientation varies markedly in the flow. On the entrance side of the nozzle at $X = -0.15 \text{ mm}$, the particles tend to align with

their large faces in the direction of flow with peaks at 90° and 270° that are well-modeled as Lorentzian functions. This angular variation is typical for particles flowing in a pipe²⁴ with a uniform cross-section; however, the spatial variation of this alignment is different. At the outlet of the constriction two new peaks appear at $\Phi = 0^\circ$ and 180° as shown in Figure 4b. These new peaks arise from particles that are oriented with their normal to the large face parallel to the overall flow direction. The peaks at 90° and 270° have approximately the same intensity as on the entrance side of the nozzle shown in Figure 4a. The intensity of the peaks at 0° and 180° is, however, much higher than those at 90° and 270° . This can be understood as all the particles that are aligned with their large face perpendicular to the flow direction would satisfy the condition that diffraction is observed on the detector and thus contribute to the intensity at 0° and 180° . However, only a small fraction of the particles that are aligned with their large face parallel to the flow direction satisfy the Bragg condition because of the cylindrical symmetry of the pipe, and so the peak intensity at 90° and 270° is less compared to that for 0° and 180° .

Figure 4c shows the intensity distribution from a position on the outlet side but below the nozzle. Only two peaks appeared at 0° and 180° , and this suggests that the particles are oriented with their large faces perpendicular to the overall flow direction near the wall. In order to understand the origin of this orientation, it is useful to consider the extent to which different regions of the flow are sampled as the pipe is scanned through the beam. The path length of the beam across the flat surface at the nozzle opening increases from the center of the pipe ($Z = 0 \text{ mm}$) to the edge of the nozzle ($Z = \pm 1 \text{ mm}$) and then decreases to zero at the edges of the pipe. This variation is shown in Figure S2 of the Supporting Information. The diffracted intensity at $\Phi = 0^\circ$ and 180° normalized by the length of the flat surface in the beam direction at the cone outlet overlaps well at different positions along the Z -axis between $\pm 1 \text{ mm}$ as shown in Figure S3 of the Supporting Information. This suggests that the orientation of the particles with their large faces perpendicular to the flow direction comes from particles parallel to the vertical wall at the exit of the nozzle. The relative intensity of the different peaks in each

region is discussed further below in connection with plots of data that are normalized with respect to the path length through the sample.

Comparison with a Fluid Dynamics Calculations. An order parameter S_2 has been calculated to quantify the alignment of particles under flow in a uniform pipe in our previous work²⁴ where the particles have shown a single alignment with respect to a director, D , parallel to the overall flow direction. S_2 is based on the second-order Legendre polynomial.³³ For a perfectly aligned sample, the maximum value is 1 as the diffracted intensity will be restricted to two points on a line defined by the director. If there is no preferential orientation, the order parameter is 0.25. As discussed above, the selection of the director is different in the cone and S_{2L} is calculated about the individual flow direction for each diffraction pattern. This selection of the director has also been used in small-angle neutron scattering studies of Ni(OH)_2 particles²² and mixtures³⁴ under elongational flow in an opposing jet cell. The values of S_{2L} are plotted in Figure 5a for each diffraction pattern in the cone. The length of the line represents the magnitude of S_{2L} and its orientation is the director at the position of measurement. The maximum value of S_{2L} calculated from the diffraction pattern is 0.88 and the minimum value is 0.26. The length of the line is proportional to the S_{2L} between these maximum and minimum values. The central region of the detector for each position of the measurement in the cone of the pipe is shown in Figure S4 of the Supporting Information. The area selected for analysis is shown with a gray scale. The regions of highest intensity are white, and the shadow of the beam stop that protects the detector from the direct beam is shown in black. The changes in the arcs of intensity for the 001 Bragg peak are immediately apparent and indicate clearly the different directions of orientation.

The alignment of kaolinite particles shown in Figure 5a can be compared with the fluid dynamics calculations in Figure 5b. A finite element computational package, COMSOL Multiphysics,³⁵ was used for the calculations. The particle volume fraction was taken as 0.03, which corresponds to the sample used, and thus the viscosity of the sample is slightly greater than that of water. The software allows us to calculate flow patterns for an incompressible Newtonian fluid in a pipe with a nozzle. The average flow velocity at the inlet and outlet of the pipe was calculated from the overall flow rate. These are 0.2 and 0.25 m s⁻¹, respectively. The sample does not show significant shear thinning and the simulations were observed to be insensitive to small changes in viscosity. The flow pattern shown in Figure 5b assumes a “no slip” boundary condition at the wall of the pipe. The arrows in the figure are along the local flow direction and the length of each arrow is proportional to the local velocity of the sample at each position, which increases from 0.2 to 1.6 m s⁻¹ at the nozzle. The data from the simulation enable us to estimate the extensional strain rate, $d\nu/dX$. Extensional strain is present throughout the conical region of the constriction where the flow is converging and is at a maximum along the axis of the pipe. The maximum extensional strain rate is about 600 s⁻¹.

The shorter length of the lines at the inlet to the cone in Figure 5a indicates that the alignment increases in the cone. S_{2L} is largest on the axis and near the walls of the cone. The order parameter increases along the axis from the inlet to the nozzle opening. The average transit time through the nozzle for a particle on the axis is about 3.3 ms. Such a particle experiences

an approximately constant elongational strain rate as the local velocity increases linearly along the cone axis as shown in Figure 5b. The increase in S_{2L} in the cone and along the axis could depend on either the local velocity or the residence time for which the particles experience a constant extensional strain and the alignment increases. The alignment is high near the walls and this cannot depend simply on the local velocity, which is zero at the walls.

The red lines at the outlet of the cone opening in Figure 5a are the regions where two extra peaks at 0° and 180° are observed and multiple directions of alignment are present with four peaks as shown in Figure 4b. It is important to note that the intensity is dominated by the peaks at 0° and 180°. The value of S_{2L} alone is not sufficient to quantify this alignment. As the algorithm that selects the director finds the maximum intensity on ring of 001 diffraction, the local director is perpendicular to the overall flow direction. The calculation of S_{2L} includes the intensity from all four peaks. The peaks at 90° and 270° reduce the calculated S_{2L} , and the lengths of the red lines are short. The red lines above and below the nozzle opening are slightly longer than the lines at the opening. The intensity variation with Φ for one of these positions has been shown in Figure 4c, and it has only two peaks at 0° and 180°. The local velocity is almost zero, and the alignment appears to be due to effects of the wall. As mentioned previously, in the central part of the pipe, regions with both nozzle opening and wall are sampled and this explains the presence of the four peaks in Figure 4b.

Dimensionless groups are often useful to identify characteristics of the behavior of a fluid flow. At a microscopic level, the orientation of particles in a dispersion is likely to occur when the strain energy associated with the flow is larger than the thermal energy of the particles. The Peclet number, Pe , is a function of these variables and for shear is taken as

$$Pe = 6\pi\eta a^3\dot{\gamma}/k_B T$$

where η is the dynamic shear viscosity, a is a characteristic dimension of the particle, $\dot{\gamma}$ is the shear strain rate, and $k_B T$ is the thermal energy. An analogous expression can be written for elongational flow that would replace shear viscosity and shear strain rate with elongational viscosity and the elongational strain rate. Reorientation is sometimes discussed using a rotational Peclet number defined as³⁶

$$P_{\text{rot}} = \dot{\gamma}/D_r$$

where D_r is the rotational diffusion coefficient that for a plate-like particle of radius R is approximately

$$D_r = 3k_B T/32\eta R^3$$

The rotational Peclet is thus smaller than Pe by the small numerical factor of $(2/9\pi)$ if the dimension a were taken as the diameter. However, given the range of sizes of particles, the order of magnitude should be considered rather than small differences.

In general, if the Peclet number is greater than unity, the energy of the flow field dominates, and it is to be expected that the structure of a fluid could be distorted and particles aligned. At the exit from the nozzle, the value of Pe reaches over 10^4 for a fluid viscosity of about 0.01 Pa s.

The Reynolds number relates the inertia of a flowing fluid and a characteristic dimension of the flow geometry to the viscosity. It can be defined as the ratio of the viscous stress to

the inertial pressure. It provides a useful indication as to when vortices or turbulence may arise. It is conventionally defined for flow in a pipe as

$$Re = \rho v d / \eta$$

where ρ is the density, v is the flow velocity, and d is the diameter of the pipe. For the density of $1.0 \times 10^3 \text{ kg m}^{-3}$, average flow velocity of 1.6 m s^{-1} , and 2 mm diameter nozzle, the Reynolds number is about 320 at the outlet of the nozzle where it changes abruptly.

The experimental conditions therefore provide high Peclet number and a modest Reynolds number for the dilute dispersion that was studied. This Reynolds number is consistent with the onset of vortices in the flow at the exit of the jet. Instabilities in flow through microchannels have been reported during polymer chain scission studies for a Reynolds number of 370.³⁷

Behavior of the Dispersion at the Nozzle Opening.

The region shown by the red lines in Figure 5a is the region where the multiple influences of alignment are significant. In this section, we discuss the effects of the constriction on the alignment of the particles over the very narrow region around its opening. The intensity normalized for sample (chord) length averaged over Φ in the nozzle and up to 0.5 mm away from its opening is shown in Figure 6.

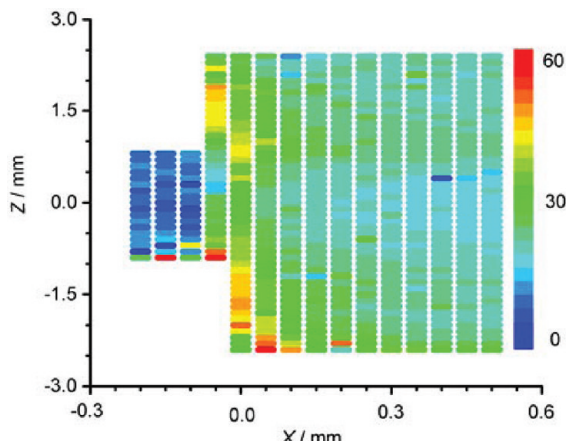


Figure 6. Chord-normalized 001 intensity averaged over Φ for each diffraction pattern of a fine raster scan around the nozzle opening. The variation of intensity shows the strong effects of the constriction on alignment over a small region. The regions of aluminum above and below the nozzle are masked in the analysis and are shown as white.

The variations in the intensity are significant in the nozzle and up to 0.15 mm from the opening. As mentioned above, the average intensity is insufficient to quantify the extent of alignment of the particles, but it suggests that the changes occur very close to the nozzle and do not extend over a large region. In Figure 6, the regions of aluminum, shown as white, are not identical above and below the nozzle because of a slight tilt in the mounting of the pipe. The pipe was found to be at about 1.15° from the horizontal. The zero position of translation in the horizontal direction was offset by 0.05 mm. The tilt and offset were constant during the period of the experiment and do not have any effect on the measurements at the constriction.

Intensity Distribution $I(\Phi)$ along the Axis. The distribution of intensity of the 001 kaolinite diffraction ring as a function of Φ along the axis of the pipe through the nozzle is shown in

Figure 7. The different azimuthal angles are shown on the vertical axis, and the colors in the spectrum indicate the variation in the intensity of the 001 diffraction.

The regions of higher intensity are red in the map. The high intensity peaks appear at $\Phi = 0^\circ$ and 180° in a very narrow region because of the clay particles near the flat surface at the exit of the nozzle opening and indicate that the large faces of the particles are perpendicular to the overall flow direction in this region. The peaks at 90° and 270° are approximately constant in intensity and show that there is a constant alignment of particles with the flow. Multiple directions of alignment are seen only very close to the nozzle and do not extend over a large region.

Variation of Averaged Normalized Intensity of the Peaks from the Particles Parallel and Perpendicular to the Flow. It is helpful to explore the spatial distribution of alignment at the nozzle outlet and by considering the intensity of diffraction in specific azimuthal directions. The average intensity for $\Phi = 90^\circ \pm 5^\circ$ and $270^\circ \pm 5^\circ$ as well as for $\Phi = 0^\circ \pm 5^\circ$ and $180^\circ \pm 5^\circ$, normalized with the total intensity for all Φ for the 001 diffraction ring is shown in Figures 8a and 8b, respectively.

The map in Figure 8a shows the intensity from particles that are aligned with their diameters parallel to the overall flow direction. Within the nozzle the particles are aligned uniformly, and there is little variation across the diameter of the constriction because of the combination of elongational and shear strains. In Figure 8b the intensity for particles that are perpendicular to the overall flow direction is seen. There are two significant effects: the data show a region where the particles are sitting at the wall at the exit of the nozzle and the overall pattern of flow that diverges away from the nozzle. The effects of the wall are significant only for a very narrow region of about 0.1 mm. The lower intensity above and below the nozzle in the region of divergent flow extends to about 0.5 mm. The differences between the areas above and below the nozzle are probably due to the tendency of the kaolinite to sediment; this effect is particularly marked in regions where the flow velocity is low.

Extent of Alignment in Terms of Order Parameter, S_2 . The order parameters, S_2 , calculated with respect to a fixed horizontal director for every position are shown for the fine scan near the nozzle in Figure 9a. The variation of S_2 as a function of the vertical coordinate, Z , for three different horizontal positions is plotted in Figure 9b. These values of S_2 should be distinguished from those for S_{2L} presented in Figure 5a where the director is chosen to be parallel to the local flow direction. The calculation of S_2 with respect to a fixed director allows us to estimate the relative amount of alignment of particles with their large faces parallel and perpendicular to the flow direction. The average velocity, 1.6 m s^{-1} , of the dispersion at the 2 mm opening is similar to that for the flow in the 5 mm uniform pipe, 1.3 m s^{-1} , described in our previous article.²⁴ In contrast, orientation for flow in a uniform pipe that shows a variation across the diameter, S_2 is approximately constant across the nozzle with a value of about 0.88. S_2 was observed to decrease from 0.9 near the wall to 0.3 at the axis of the pipe in the uniform pipe.²⁴ The variation of velocity along the flow direction provides a constant extensional strain rate that has a maximum value equal to 600 s^{-1} on the horizontal axis. The shear strain rate will be a minimum on this axis. The effects of the extensional strain rate are dominant on the axis and decrease toward the walls while the influence of shear strain increases from the axis to the walls. This combination of

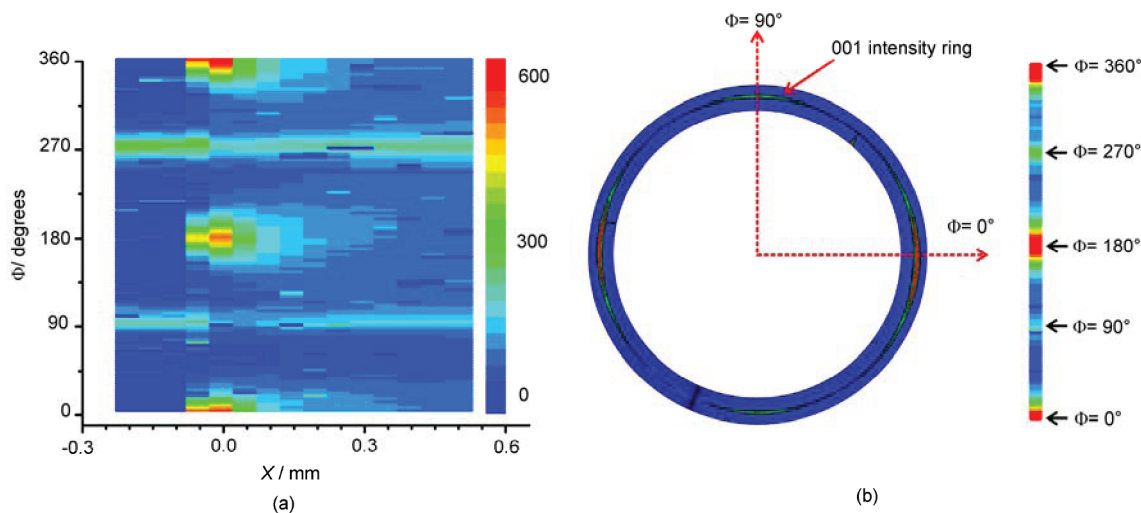


Figure 7. (a) The 001 diffracted intensity variation with azimuthal angle for points along the axis of the pipe. Data is chord-normalized to allow for the different amounts of sample in the beam. The red spots represent the peaks at 0° and 180° which appear as the plate-like particles orient with their large face perpendicular to the flow direction on the walls at the exit of the nozzle. (b) The 001 diffraction peak for $X = 0.0$ mm and $Z = 0.0$ mm is presented as it appears on the detector.

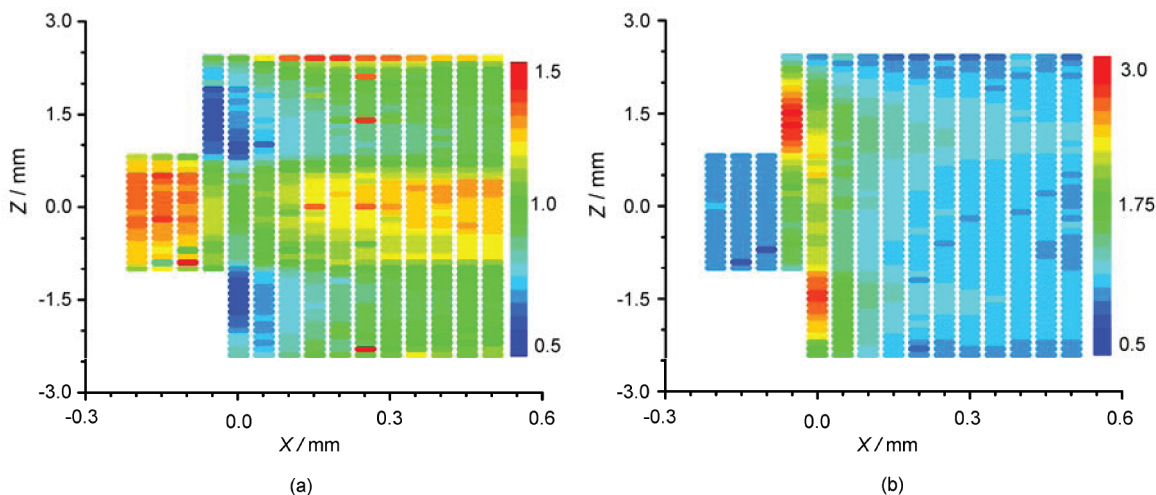


Figure 8. Normalized intensity for the 001 Bragg peak at specific azimuthal angles. Data for (a) $\Phi = 90 \pm 5^\circ$ and $270 \pm 5^\circ$ and (b) $0 \pm 5^\circ$ and $\Phi = 180 \pm 5^\circ$. In both cases, the average intensity of selected sectors is normalized by the total intensity in the 001 diffraction peaks.

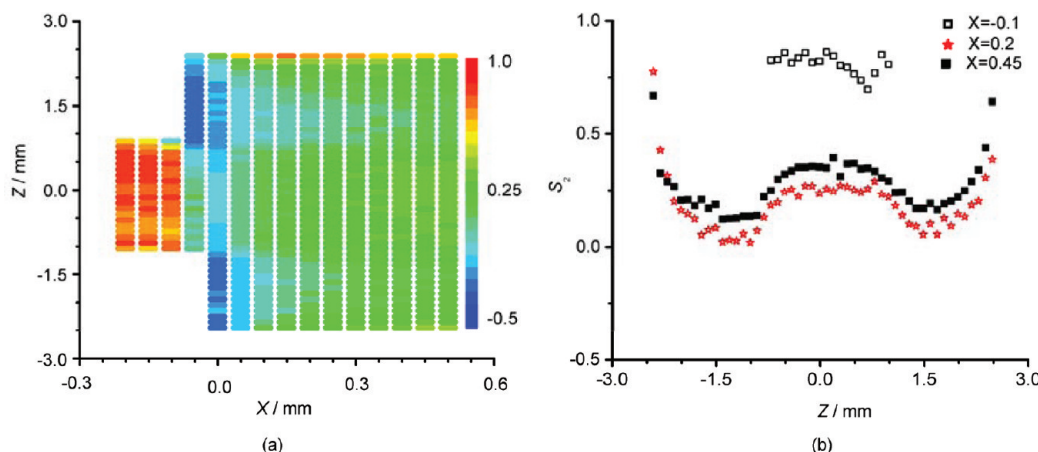


Figure 9. (a) Order parameter, S_2 , for each diffraction pattern. (b) S_2 versus Z at different X positions across the pipe. Higher values of S_2 in the nozzle at $X = -0.1$ mm decreases at $X = 0.0$ mm and goes to less than 0.25 where the particles rotate 90° . S_2 increases as we move away from the nozzle opening. The errors that arise from counting statistics are smaller than the plotted data points.

extensional and shear strain induces a high degree of uniform orientation for particles flowing through the nozzle. The extensional strain is not present in the uniform straight pipe and the alignment arises only from the shear that is less at the center of the pipe.

There are only a few other studies with which the data that we have presented here for quantitative measures of orientation can be compared. The effects of elongational strain have been described for similar sized plate-like objects that are formed from a lamellar surfactant phase.³⁴ The extensional strain rate in the cone is much higher, up to 600 s^{-1} , than that in the opposed jet cell of about 6 s^{-1} . However, the sample concentration was about 15 vol %, and a high degree of alignment was observed. Studies with smaller disk-like particles²² have shown that the volume fraction is an important parameter, and so comparison between different studies must carefully consider aspect ratio, size, and volume fraction.

In Figure 9a, the regions that are shown in blue have values of S_2 that are less than 0.25, which is the value for a uniform ring of intensity. As the order parameter is calculated with respect to a fixed director that is along the axis of the pipe, it is dominated in these regions by particles aligned perpendicular to the overall flow direction. Such orientation of particles give peaks for $\Phi = 0^\circ$ and 180° that are more intense than those aligned with the flow. In Figure 9b, the value of S_2 is uniform across the nozzle and the value of S_2 is about 0.88. S_2 decreases at $X = 0.25\text{ mm}$ and starts increase at $X = 0.45\text{ mm}$ from the nozzle as the particles re-establish their original flow orientation. In our previous studies, S_2 was about 0.9 near the walls and was not uniform across the pipe.²⁴

CONCLUSIONS

We have demonstrated that the alignment of crystalline, disk-like colloidal particles such as kaolinite dispersed in water can be measured quantitatively in complex geometries such as that found at a constriction in a pipe. Such data are important as many practical applications involve flow that is not uniform or even smoothly varying and is not dominated by shear strains. The distribution of the orientation has been determined by quantitative measurements of the intensity of particular Bragg diffraction peaks that are characteristic of specific directions of the particles.

The convergent flow geometry provides a component of elongational strain rate that has a maximum value of 600 s^{-1} in the cone. The combination of elongational and shear strain provides uniform alignment for the plate-like particles at the nozzle whereas for flow in a uniform pipe the orientation was higher near the walls and not uniform across the pipe. The microscopic behavior is understood in the light of the fluid mechanics simulations that indicate a Peclet number, several thousand, that is high at exit of the jet and an abrupt change in the Reynolds that is of the order of a hundred. The orientation distribution in the circular section pipe was found to be a Lorentzian. In uniform flow, the disk-like particles are aligned strongly with their long dimension, the diameter, parallel to the flow direction. Surprisingly, at the exit of the constriction, there is an apparent region of the flow where the plate-like particles are oriented with their long dimension perpendicular to the overall flow, and two extra peaks are observed. This realignment is observed only within about 0.15 mm of the nozzle. In the same region, there is a reduction of particles aligned parallel to the flow. The intensity of these extra peaks scale in proportion to the path length of the beam along the flat

wall that is perpendicular to the flow, and so it can be concluded that this is an effect of these walls and the overall flow geometry that creates stable vortices rather than local turbulence or unusual alignment of particles in a flow field. Further from the constriction, the original flow pattern for a uniform pipe is re-established.

Diffraction data can be analyzed to provide a quantitative measure of the orientation that can be compared with models. The sample in these experiments had a low volume fraction and a simple fluid dynamics calculation gives a reasonable estimate of the velocity distribution in the flow geometry. The calculations show that there is high shear strain at the edges of the conical restriction and that there is elongational strain in the cone. These account well for the strong alignment parallel to the flow at the entrance to the nozzle. The orientation can be represented as spatial maps of the order parameter S_2 that is obtained from the average of the data with a Legendre polynomial. The measured values of S_2 and the calculated velocity patterns in the cone inlet correlate well. On the outlet side of the nozzle, there is alignment of particles parallel to the wall of the constriction in regions where the velocity is expected to be very low.

A Lorentzian distribution is not well represented by the Legendre polynomial P_2 , but the magnitude of S_2 or S_{2L} is still a useful parameter when there is a single axis of orientation. In principle, S_2 can be compared directly with measurements by other techniques such as nuclear magnetic resonance or optical birefringence that provide only this average parameter. In regions of flow where multiple orientations are observed, the single parameter S_2 is not adequate, and to provide a complete description of the orientation, functions with more parameters are needed. To a limited extent, higher order parameters such as S_4 are useful, but full maps of the distribution are highly advantageous.

The experiments have demonstrated that even in macroscopic flow geometries with dimensions of order millimeters, high spatial resolution at scales smaller than $100\text{ }\mu\text{m}$ is necessary in order to observe the changes in flow. Diffraction with focused synchrotron X-ray beams is valuable for such studies and experiments can be conducted with a range of flow geometries and samples. These can include samples with nonlinear rheological properties such as concentrated dispersions and polymer composites. Experimental studies can be made of flow patterns that would be outside the scope of simulations.

ASSOCIATED CONTENT

Supporting Information

Typical full raw diffraction images corresponding to data shown in Figure S1; variations of the amount flat surface at the nozzle outlet against position along the vertical axis (Figure S2); intensity normalized by the length of flat surface as a function of azimuthal angle Φ for the different positions at the exit of the nozzle (Figure S3); a map of the diffraction patterns showing the 001 diffraction rings for the various positions in the nozzle (Figure S4). This material is available free of charge via the Internet at <http://pubs.acs.org>.

AUTHOR INFORMATION

Corresponding Author

*E-mail: Junaid.Qazi@live.com.

Present Address

[‡]Pulp and Paper Centre, University of British Columbia, 2385 East Mall, Vancouver, Canada.

Notes

The authors declare no competing financial interest.

[†]On study leave from COMSATS Institute of Information Technology, Pakistan.

ACKNOWLEDGMENTS

We are very grateful to Paul Stukas for construction of the pipe and nozzle. Martin Vickers is thanked for help in preparing the experiment and pump system. Dr. Jon Wright assisted with the operation of the ID11 beamline. We thank the ESRF for an allocation of beam time. The Swedish Research Council (VR) is acknowledged for partial financial support.

REFERENCES

- (1) Calvert, P. Inkjet printing for materials and devices. *Chem. Mater.* **2001**, *13*, 3299–3305.
- (2) Kamyshny, A.; Ben-Moshe, M.; Aviezer, S.; Magdassi, S. Inkjet printing of metallic nanoparticles and microemulsions. *Macromol. Rapid Commun.* **2005**, *26*, 281–288.
- (3) Sirringhaus, H.; Kawase, T.; Friend, R. H.; Shimoda, T.; Inbasekaran, M.; Wu, W.; Woo, E. P. High-resolution inkjet printing of all-polymer transistor circuits. *Science* **2000**, *290*, 2123–2126.
- (4) Sosa, A.; Carreau, P. J.; Tanguy, P. A.; Ascanio, G.; Guerrero, C. The effect of thickener on the rheology of coating colors. *Chem. Eng. Commun.* **2006**, *193*, 917–928.
- (5) Li, J.; Tanguy, P. A.; Carreau, P. J.; Moan, M. Effect of thickener structure on paper-coating color properties. *Colloid Polym. Sci.* **2001**, *279*, 865–871.
- (6) Coussot, P. Rheophysics of pastes: a review of microscopic modelling approaches. *Soft Matter* **2007**, *3*, 528–540.
- (7) Vermant, J.; Solomon, M. J. Flow-induced structure in colloidal suspensions. *J. Phys.: Condens. Matter* **2005**, *17*, R187–R216.
- (8) Malkin, A. Ya.; Semakov, A. V.; Kulichikhin, V. G. Self-organization in the flow of complex fluids (colloid and polymer systems) Part 1: Experimental evidence. *Adv. Colloid Interface Sci.* **2010**, *157*, 75–90.
- (9) Ashdown, S.; Marković, I.; Ottewill, R. H.; Lindner, P.; Oberthür, R. C.; Rennie, A. R. Small-angle neutron-scattering studies on ordered polymer colloid dispersions. *Langmuir* **1990**, *6*, 303–307.
- (10) Ackerson, B. J.; Clark, N. A. Shear-induced partial translational ordering of a colloidal solid. *Phys. Rev. A* **1984**, *30*, 906–918.
- (11) Ackerson, B. J.; Clark, N. A. Sheared colloidal suspensions. *Physica A* **1983**, *118*, 221–249.
- (12) Ramsay, J. D. F.; Lindner, P. Small-angle neutron scattering investigations of the structure of thixotropic dispersions of smectite clay colloids. *J. Chem. Soc., Faraday Trans.* **1993**, *89*, 4207–4214.
- (13) Bihannic, I.; Baravian, C.; Duval, J. F. L.; Paineau, E.; Meneau, F.; Levitz, P.; de Silva, J. P.; Davidson, P.; Michot, L. J. Orientational order of colloidal disk-shaped particles under shear-flow conditions: a rheological small-angle X-ray scattering study. *J. Phys. Chem. B* **2010**, *114*, 16347–16355.
- (14) Rennie, A. R.; Bare, S.; Cockcroft, J. K.; Jupe, A. C. Characterization of the flow of anisotropic colloidal particles using energy-dispersive X-ray diffraction. *J. Colloid Interface Sci.* **2006**, *293*, 475–482.
- (15) Clarke, S. M.; Rennie, A. R.; Convert, P. A diffraction technique to investigate the orientational alignment of anisotropic particles: studies of clay under flow. *Europhys. Lett.* **1996**, *35*, 233–238.
- (16) Jogun, S. M.; Zukoski, C. F. Rheology and microstructure of dense suspensions of plate-shaped colloidal particles. *J. Rheol.* **1999**, *43*, 847–871.
- (17) Barè, S.; Cockcroft, J. K.; Colston, S. L.; Jupe, A. C.; Rennie, A. R. X-ray study of the orientational order of a concentrated dispersion of kaolinite under flow. *J. Appl. Crystallogr.* **2001**, *34*, 573–579.
- (18) Goodwin, J. W.; Hughes, R. W. *Rheology for Chemists—an Introduction*; Royal Society of Chemistry: Cambridge, 2000.
- (19) Barnes, H. A.; Hutton, J. F.; Walters, K. *Introduction to Rheology*; Elsevier: Amsterdam, 1989.
- (20) Penfold, J.; Tucker, I. Flow-induced effects in mixed surfactant mesophases. *J. Phys. Chem. B* **2007**, *111*, 9496–9503.
- (21) Penfold, J.; Staples, E.; Tucker, I.; Carroll, P.; Clayton, J.; Cowan, J. S.; Lawton, G.; Amin, S.; Ferrante, A.; Ruddock, H. Elongational flow induced ordering in surfactant micelles and mesophases. *J. Phys. Chem. B* **2006**, *110*, 1073–1082.
- (22) Qazi, S. J. S.; Rennie, A. R.; Tucker, I.; Penfold, J.; Grillo, I. Alignment of dispersions of plate-like colloidal particles of $\text{Ni}(\text{OH})_2$ induced by elongational flow. *J. Phys. Chem. B* **2011**, *115*, 3271–3280.
- (23) Brown, A. B. D.; Rennie, A. R. Monodisperse colloidal plates under shear. *Phys. Rev. E* **2000**, *62*, 851–862.
- (24) Qazi, S. J. S.; Rennie, A. R.; Wright, J. P.; Cockcroft, J. K. Alignment of plate-like particles in a colloidal dispersion under flow in a uniform pipe studied by high-energy X-ray diffraction. *Langmuir* **2010**, *26*, 18701–18709.
- (25) Chandrasekhar, S. *Liquid Crystals*; Cambridge University Press: New York, 1980; p 42.
- (26) Ruland, W. Elimination of the effect of orientation distributions in fiber diagrams. *Colloid Polym. Sci.* **1977**, *255*, 833–836.
- (27) Lovell, R.; Mitchell, G. R. Molecular orientation distribution derived from an arbitrary reflection. *Acta Crystallogr.* **1981**, *A37*, 135–137.
- (28) Burger, C.; Ruland, W. Evaluation of equatorial orientation distributions. *J. Appl. Crystallogr.* **2006**, *39*, 889–891.
- (29) Brown, A. B. D.; Clarke, S. M.; Convert, P.; Rennie, A. R. Orientational order in concentrated dispersions of plate-like kaolinite particles under shear. *J. Rheol.* **2000**, *44*, 221–233.
- (30) van Olphen, H. *An Introduction to Clay Colloid Chemistry*; Wiley: New York, 1963.
- (31) ID11 beam line: <http://www.esrf.eu/UsersAndScience/Experiments/StructMaterials/ID11/>.
- (32) Snigirev, A.; Snigireva, I.; Vaughan, G.; Wright, J.; Rossat, M.; Bytchkov, A.; Curfs, C. High energy X-ray transfocator based on Al parabolic refractive lenses for focusing and collimation. *J. Phys. Conf. Ser.* **2009**, *186*, 012073.
- (33) Spiegel, M. R. *Mathematical Handbook of Formulas and Tables*; McGraw-Hill: New York, 1968; p 146.
- (34) Qazi, S. J. S.; Rennie, A. R.; Tucker, I.; Penfold, J.; Grillo, I. Impact of $\text{Ni}(\text{OH})_2$ plate-like particles on lamellar surfactant mesophases and the orientation of their mixtures under elongational flow. *J. Phys. Chem. B* **2011**, *115*, 10413–10424.
- (35) COMSOL Multiphysics version 3.5a, www.comsol.com.
- (36) Brenner, H. Rheology of a dilute suspension of axisymmetric Brownian particles. *Int. J. Multiphase Flow* **1974**, *1*, 195–341.
- (37) Vanapalli, S. A.; Ceccio, S. L.; Salomon, M. J. Universal scaling for polymer chain scission in turbulence. *Proc. Natl. Acad. Sci. U. S. A.* **2006**, *7*, 16660–16665.

Orientation of a Dispersion of Kaolinite Flowing in a Jet

Supporting Information

S. Junaid S. Qazi, Adrian R. Rennie, Jeremy K. Cockcroft

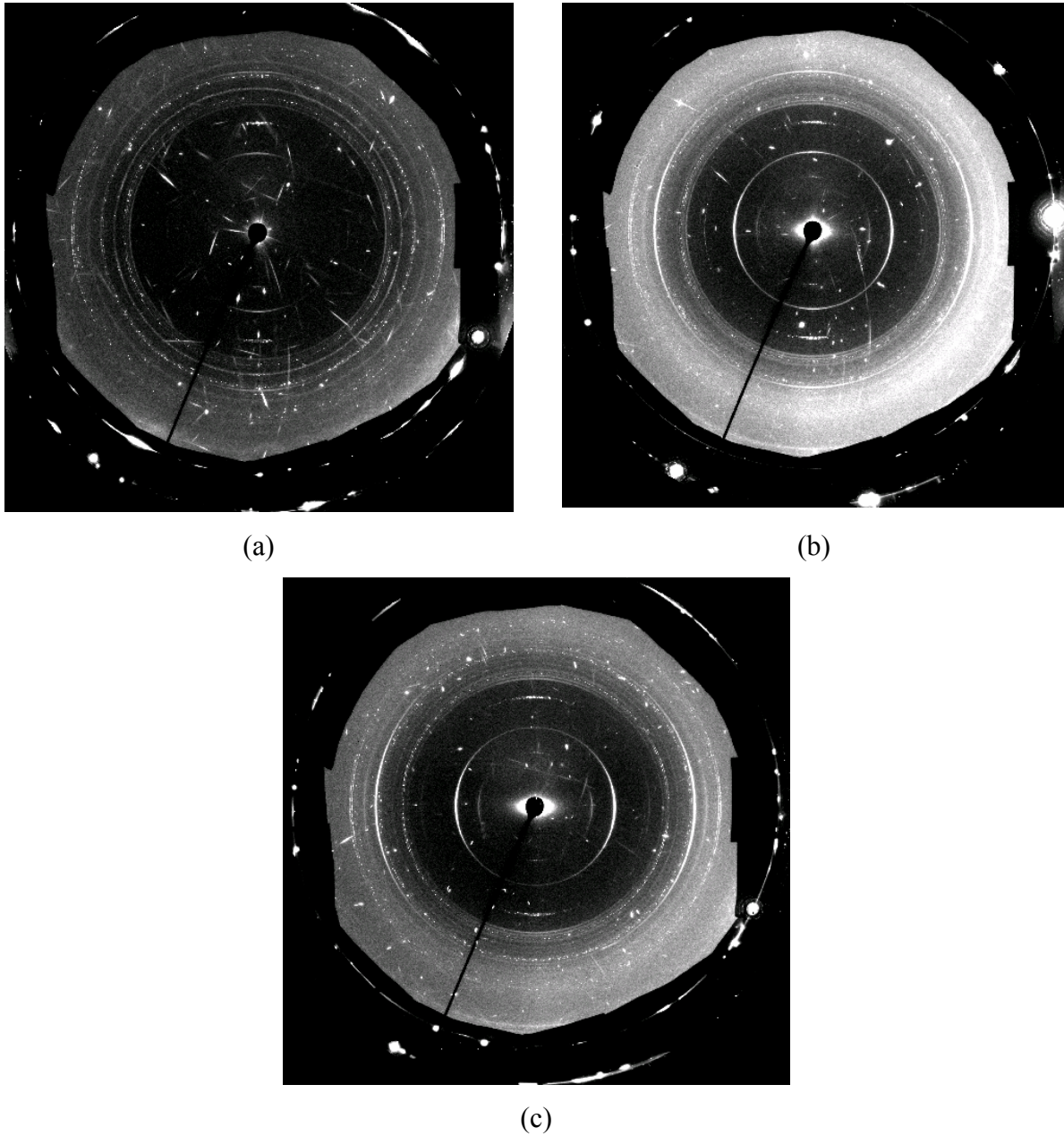


Figure S1. Complete raw data diffraction patterns at the three different positions in a pipe shown in Figure 4. (a) At $X = -0.15$ mm, $Z = 0.0$ mm, (b) At the nozzle opening, $X = 0.0$ mm, $Z = 0.0$ mm, (c) At $X = 0.05$ mm, $Z = -1.8$ mm. Intensity distributions for these diffraction patterns, as a function of azimuthal angle, for the 001 ring are shown in Figures 4 (a) (b) and (c), respectively, in the main article. The other peaks in these patterns could be analyzed to provide more extensive data about the three-dimensional orientation.

These diffraction patterns show that the measured data includes, apart from several diffraction peaks from the kaolinite particles, sharp and very intense single-crystal diffraction spots from individual grains of aluminum, which also results in multiple scattering from aluminum, as well as diffuse scattering from water.

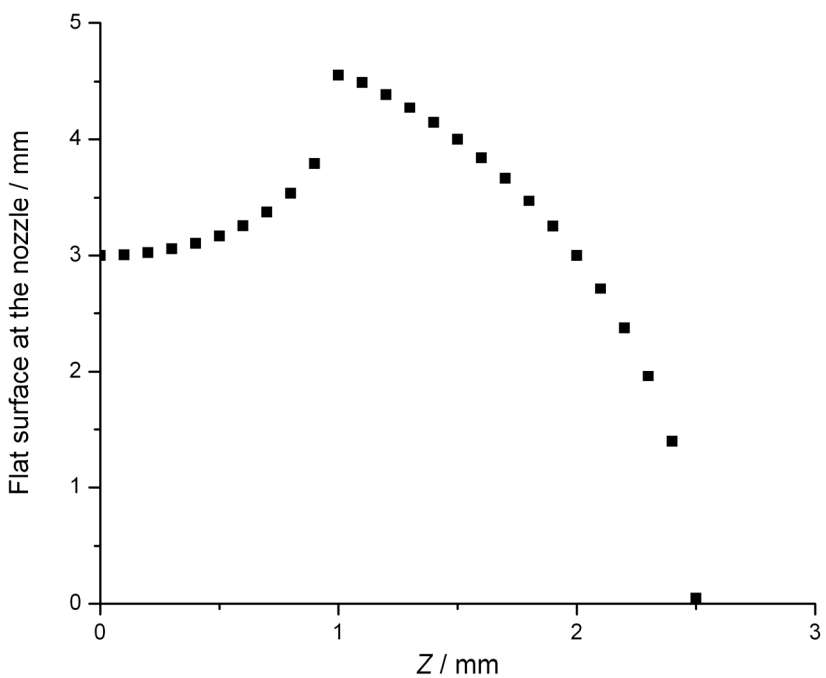


Figure S2. The path length of the beam along the flat surface at the nozzle opening increases from the centre of the pipe to the nozzle edge and then decreases to zero at the wall. The length of the flat surface is identical to the chord length that represents the entire sample thickness above and below the nozzle ($Z > \pm 1$ mm).

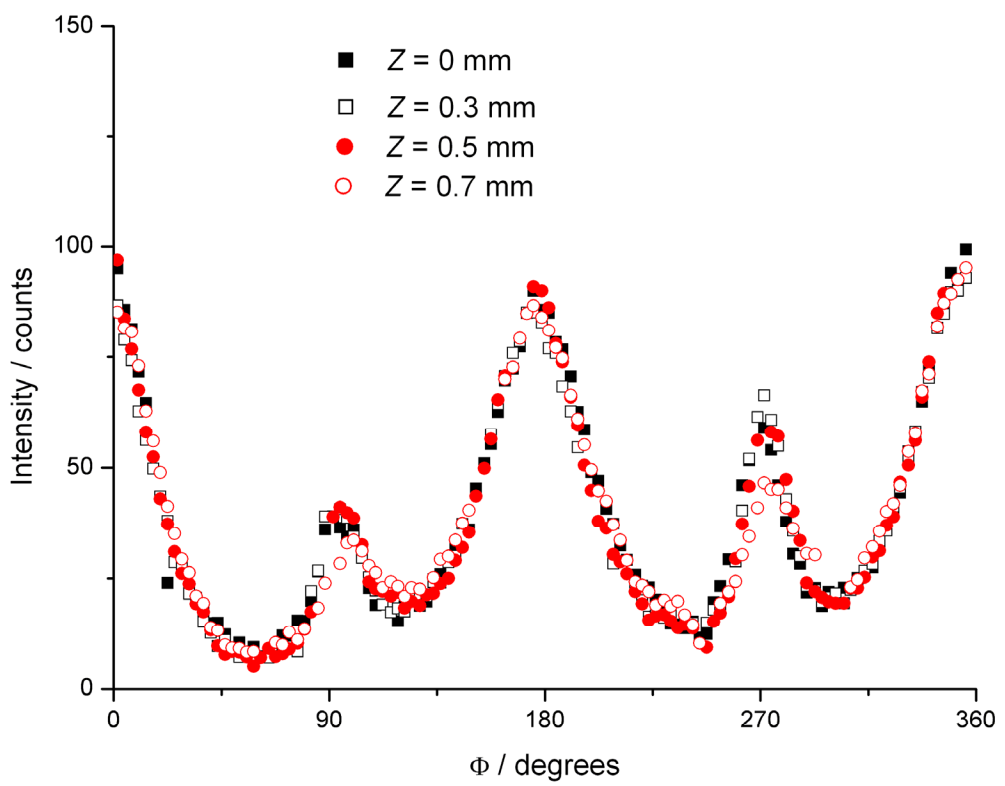


Figure S3. The intensity is normalized by the length of the flat surface along the beam direction at the nozzle outlet. The peaks match up very well across the pipe opposite to the nozzle opening at different positions of measurements.

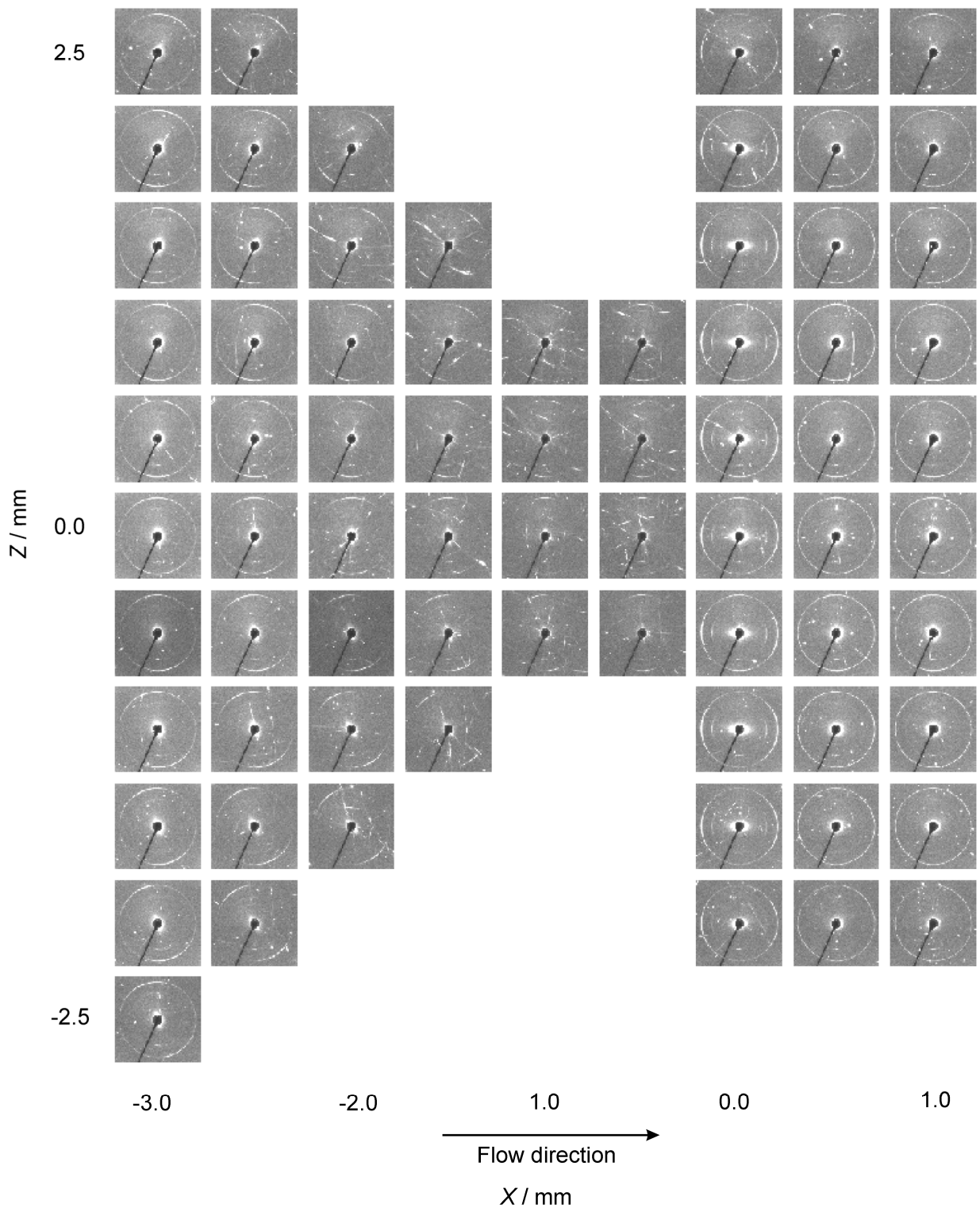


Figure S4. Diffraction patterns in the cone and at the nozzle opening. Clay particles are more aligned as they come closer to the nozzle opening. Four peaks at 001 intensity ring appear at the nozzle opening which shows that a fraction of particles are aligned 90° to the flow direction.